ACS APPLIED MATERIALS & INTERFACES

www.acsami.org

Research Article

Ultrastable Anion Radicals in Ligand-Dimerized Frameworks for Self-Accumulated Electrochemiluminescence

Qizhou Chen,[§] Yuming Gu,[§] Haomin Fu,[§] Rengan Luo, Da Zhu, Pengfei Dong, Jing Ma,* Huangxian Ju, and Jianping Lei*

Cite This: *ACS Appl. Mater. Interfaces* 2024, 16, 18194−18201

Read Online

ACCESS | Metrics & More | Article Recommendations | Supporting Information

ABSTRACT: Electrochemiluminescence (ECL) is a light-emitting process that occurs via an annihilation reaction among energetic radical intermediates, whose stabilities determine the ECL efficiency. In this study, a ligand-dimerized metal−organic framework (MOF) with ultrastable anion radical is designed as an efficient nanoemitter for self-accumulated ECL. Due to the nonplanar structure of perylene diimide (PDI) derivate, two PDI ligands in the framework form a J-dimer unit with a vertical distance of ∼5.74 Å. In cathodic scanning, the ligand-dimerized MOF demonstrates three-step ECL emissions with a gradual increase in ECL intensity. Unlike the decrease in the PDI ligand, the self-accumulated ECL of the MOF was observed with 16.8-fold enhancement due to the excellent stability of radical intermediates in frameworks. Electron paramagnetic resonance demonstrated the ultrastability of free radicals in the designed frameworks, with 82.2% remaining even after one month of storage. Density functional theory calculations supported that PDI dimerization was energetically favorable upon successive electron injection. Moreover, the ECL wavelength is 610 nm, corresponding to the emission of excited dimers. The radical-stabilized reticular nanoemitters open up a new platform for decoding the fundamentals of self-accumulated ECL systems.

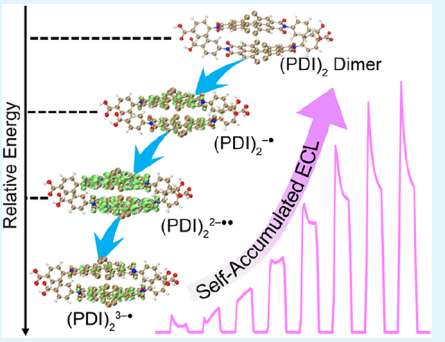

KEYWORDS: *metal−organic frameworks, electrochemiluminescence, anion radical, mechanism, electrochemistry*

INTRODUCTION

Electrochemiluminescence (ECL) is an optoelectronic transduction process involving the electrochemically generated energetic radicals on the electrode surface, which subsequently annihilate each other to generate excited states for ECL emission.[1−4] However, unstable radical intermediates in conventional emitters are usually consumed in detection environments, especially in aqueous solution, prior to the ECL reaction, leading to the low ECL efficiency. To reduce the consumption, most of approaches are based on the accelerated charge transfer between radical intermediates,[5,6] thereby improving the ECL system's efficiency.[7,8] Typically, the integrating luminophores with the coreactants in a single structural unit shortens the reaction path[9,10] and thus accelerates the charge transfer to enhance the ECL.[11,12] A donor−acceptor framework is designed as the nanoemitter to promote electron transfer via intrareticular charge transfer pathway for radical complexation, resulting in a robust ECL.[13,14] Alternatively, the improvement of the energetic radical cations/anions' stability on the electrode surface could be a promising way to enhance the strength of ECL emission.[15,16]

To improve the stability of free radicals,[17−19] one common approach is to shield the radicals by introducing large substituents,[20−22] and another is to increase the delocalized nature of unpaired electrons on the molecular backbone.[23,24] Metal−organic frameworks (MOF) are a type of porous crystalline materials with strict skeleton and designable ligands.[25] Introducing the conjugated ligands into MOFs can effectively improve the stability of radical intermediates owing to the rigid structure and shielding effect of frameworks.[26−28] For example, MOFs containing naphthalenediimides realized radical stabilization through the electron delocalization and spin-pairing of an *in situ* coplanar dimer structure within the framework.[29] Perylene diimide (PDI) derivates with large conjugated structures have excellent electron-accepting ability to generate delocalized anion radicals in frameworks,[30−33] giving a perspective in ECL applications.

Inspired by the framework-promoted radical stabilization, we utilized Ni^{2+} as a node and N,N′-di(4-benzoic acid)-1,2,6,7-tetrachloroperylene-3,4,9,10-tetracarboxylic acid diimide (a PDI derivate) as a ligand, which formed a J-dimer in the frameworks. In the cathodic scanning, three-step ECL

Received: January 24, 2024
Revised: March 12, 2024
Accepted: March 13, 2024
Published: March 27, 2024

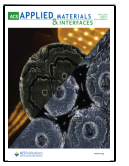

https://doi.org/10.1021/acsami.4c01412
ACS Appl. Mater. Interfaces 2024, 16, 18194−18201

emissions were observed. Moreover, the transient ECL of MOF demonstrated 16.8-fold enhancement upon successive tests, resulting in the self-accumulated ECL. According to density functional theory (DFT) calculations of the PDI dimer in frameworks, the designed MOF demonstrated a gradual decrease of energy upon electron injection, which makes electrochemically generated radical intermediates much more stable to promote the production of excited states. Electron paramagnetic resonance (EPR) further identified the one-month stability of free radicals in frameworks, facilitating the radical accumulation during the ECL process. Compared with conventional ECL nanoemitters, the MOF emitters with stabilized radicals effectively accelerated the generation of excited states during the ECL process, which greatly improved the ECL efficiency and stability. To the best of our knowledge, it is the first example that utilizes ligand-dimerized MOFs to produce stable radicals for self-accumulated ECL emission, enriching the ECL enhancement mechanism.

EXPERIMENTAL SECTION

Materials and Reagents. Tripropylamine (TPrA), propionic acid, 4-aminobenzoic acid, and N,N-dimethylformamide (DMF) were acquired from Sinopharm Chemical Reagent Co., Ltd. (Shanghai, China). 1,6,7,12-Tetrachloroperylene tetracarboxylic acid dianhydride was purchased from Bide Pharmatech Co., Ltd. (Shanghai, China). Nickel nitrate hexahydrate ($Ni(NO_3)_2{\cdot}6H_2O$) and potassium persulfate ($K_2S_2O_8$) were obtained from Aladdin Chemistry Co., Ltd. (Shanghai, China). Acetonitrile, tetrabutylammonium hexafluorophosphate, and nickel glycine (Ni-gly) were purchased from Macklin Biochemical Co., Ltd. (Shanghai, China). Phosphate buffer solution (PBS, 0.1 M, pH 7.4) was prepared with $NaH_2PO_4{\cdot}2H_2O$ and $Na_2HPO_4{\cdot}12H_2O$. All aqueous solutions were prepared using ultrapure water, which was obtained from a Millipore water purification system (Milli-Q, $\geq$ 18.2 MΩ cm^{-1}).

Apparatus. ^1H NMR spectra were collected on a Bruker Advance III 400 MHz spectrometer at room temperature. Powder X-ray diffraction (PXRD) data were recorded with a Bruker D8-Advance diffractometer with a Cu-sealed tube (λ = 1.54178 Å) at 40 kV and 40 mA with 0.2 s per step. Scanning electron microscopy images were taken on an S-4800 scanning electron microscope (Hitachi, Japan). Transmission electron microscopy images were taken on a JEM-2010 transmission electron microscope (JEOL, Japan). Photoluminescence (PL) spectra were measured on an FLS-980 fluorescence spectrophotometer (Edinburgh Instrument., U.K.). Infrared spectra were collected on a Vector 22 Fourier transform infrared (FT-IR) spectrometer (Bruker Optics, Germany). Ultraviolet and visible-diffuse-reflectance spectra (UV−vis DRS) were acquired on a UV-3600 UV−vis-NIR spectrophotometer (Shimadzu Co., Japan). X-ray photoelectron spectroscopy (XPS) was performed on an ESCALAB 250 spectrometer (Thermo-VG Scientific Co., U.S.A.) with ultrahigh vacuum generators.

Electron Paramagnetic Resonance. EPR measurements were performed on a Bruker BioSpin EMX PLUS (PPMS) EPR spectrometer at ambient temperature. MOF and PDI ligand were placed in two 3 mm I.D. EPR quartz sample tubes and were tested at room temperature without a trapping agent. Stability tests were performed under *in situ* light and the EPR signal was detected at fixed intervals (1 min, 30 s). When stability tests were performed, the instrument parameters for the PDI ligand and MOF were set at power (2.0 mW), power attenuation (20 dB), gain (30 dB), modulation amplitude (1.5 G), and power (0.2 mW), power attenuation (30 dB), gain (20 dB), and modulation amplitude (0.1 G). Specifically, to obtain comparable signals for both the MOF and PDI ligand, the instrument parameters were adjusted at power (2.0 mW), power attenuation (20 dB), gain (30 dB), and modulation amplitude (0.5 G).

Synthesis of PDI Ligand and MOF. N,N′-Di(4-benzoic acid)-1,2,6,7-tetrachloroperylene-3,4,9,10-tetracarboxylic acid diimide (PDI) ligand was synthesized according to a reported literature with some modifications.[28] Briefly, the mixture of 1,6,7,12-tetrachloroperylene tetracarboxylic acid dianhydride (200 mg, 0.378 mmol), aminobenzoic acid (518 mg, 3.78 mmol), and propionic acid (25 mL) were stirred at 140 °C for 48 h. After the mixture was cooled to room temperature, water was added to promote precipitation, followed by filtration and washing with a mixture of 1:1 methanol/water. Afterward, the crude product was obtained by vacuum drying overnight at room temperature. Finally, recrystallization with DMF yielded a pure crimson powder. Yield: 69%. ^1H NMR (400 MHz, DMSO): δ 13.18 (s, 1H), 8.63 (s, 2H), 8.14 (d, J = 8.0 Hz, 2H), 7.59 (d, J = 8.0 Hz, 2H). HRMS (m/z), $[M\text{-}H]^-$: Calc. 764.9431, found 764.9428 (Figures S1 and S2).

For MOF, a mixture of $Ni(NO_3)_2{\cdot}6H_2O$ (15 mg, 0.052 mmol), PDI (10 mg, 0.013 mmol), and DMF (3 mL) was heated in a Teflon-lined autoclave at 100 °C for 72 h.[34] Red powder was collected via washing with DMF and methanol several times and subsequent drying at room temperature. The structure of MOF was modeled by referring to the similar metal−organic frameworks crystal structure.[35] The lattice parameters of bulk MOF were a = 50.89 Å, b = 19.97 Å, and c = 16.31 Å. Simulated PXRD patterns of MOF were obtained from Materials Studio 2020.

Cyclic Voltammetry. Cyclic voltammetry (CV) was recorded with a CHI-630D electrochemical workstation (CHI Instruments Inc., China). All studies were performed with a conventional three-electrode system in the potential range from 0.0 to −1.9 V with a scan rate of 0.1 V s^{-1}. The working electrode in the three-electrode system is a glassy carbon electrode (GCE, d = 5 mm), and the auxiliary electrode is a platinum electrode. Specifically, Ag/AgCl and Ag/Ag^+ are utilized as the reference electrode in the aqueous and acetonitrile phases, respectively. The GCE was polished with 0.3 and 0.05 μm alumina powder, followed by ultrasonic cleaning in water, ethanol, and water for 3 min before each experiment. Finally, the cleaned electrodes were purged and dried with a high purity nitrogen. For preparation of the modified GCEs, the MOF, PDI ligand, Ni-gly, and $Ni(NO_3)_2{\cdot}6H_2O$ were individually dispersed in ultrapure water to form 1.0 mg/mL suspension, and then 20 μL of the modified suspension was evenly coated on the surface of GCEs.

ECL Measurement and Spectra. The ECL measurements were conducted on MPI-EII multifunctional electrochemical and chemiluminescent analytical system (Xi'an Remex Analytical Instrument Co., Ltd. China) with a conventional three-electrode system. All measurements were carried out in 0.1 M PBS containing 0.1 M KCl and $K_2S_2O_8$ at a 500 V photomultiplier tube (PMT), except for 900 V of stepping pulse (SP) without coreactant and 700 V of ECL measurements with 100 mM H_2O_2. The ECL spectra were measured in a home-built ECL spectroscopic analyzer consisting of a Nikon Eclipse (Ti), Princeton Instruments Acton SpectraPro SP-

https://doi.org/10.1021/acsami.4c01412
ACS Appl. Mater. Interfaces 2024, 16, 18194−18201

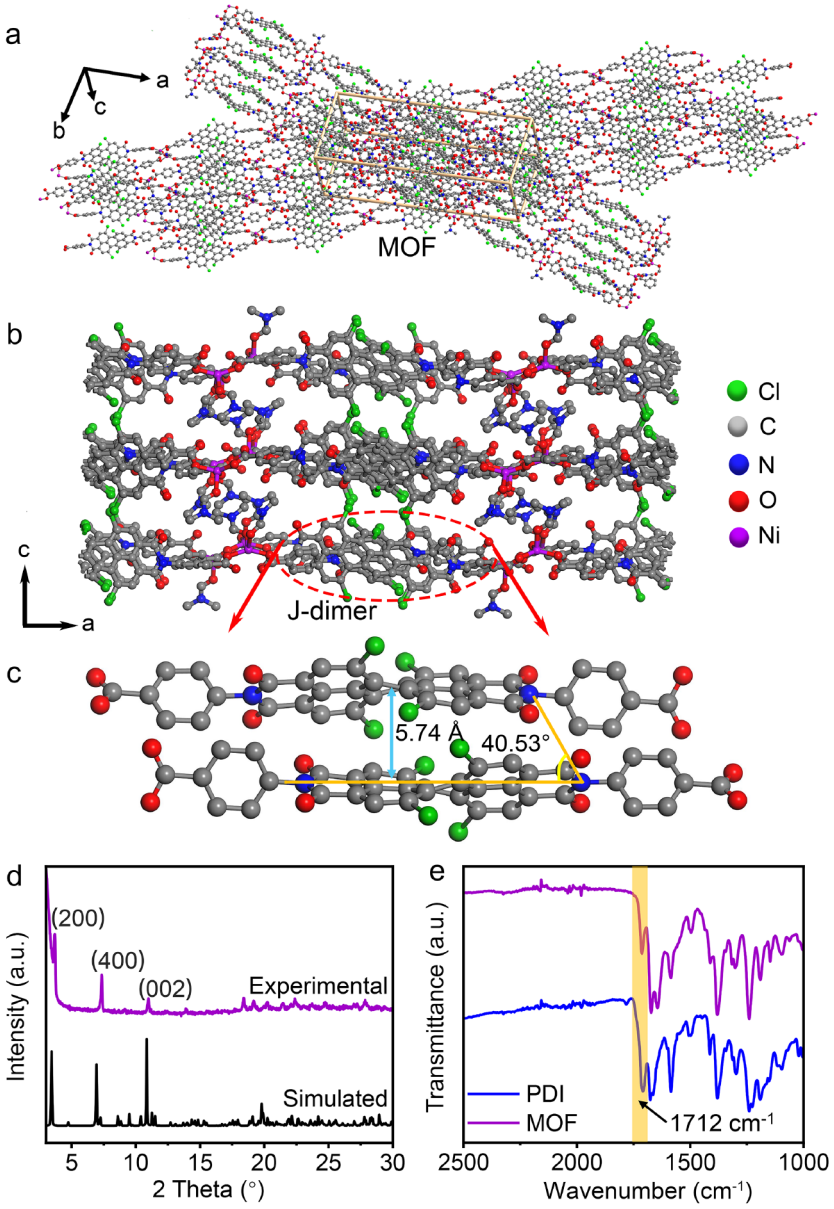

Figure 1. (A) 3D structure of MOF and (b) head-to-tail arrangement of PDI ligands in the framework along the *b*-axis. (c) Structure of PDI dimer in the framework. (d) Experimental and simulated PXRD patterns of the MOF. (e) FT-IR spectra of PDI ligand and MOF powder.

2300, Princeton Instruments PyLoN at −120 °C and a CHI-630D electrochemical workstation. The spectra of MOF-modified GCEs were collected under potential of −1.2 and −2.0 V for 30 s in 0.1 M PBS containing 100 mM $K_2S_2O_8$.

DFT Calculations. The PDI, $(PDI)_2$, and Ni-$(PDI)_2(DMF)_2$ cluster models were used in the calculations of MOF. All the DFT and time-dependent density functional theory (TD-DFT) calculations were carried out with the Guassian 16 package suite.[36] Structures were optimized by using B3LYP functional[37,38] with D3BJ empirical dispersion. The 6-31G(d) basis set was employed for C, H, O, N, and Cl atoms, while the LANL2DZ basis set, together with the related effective core potentials,[39] was used for Ni atoms. The formation energies for different reduced states of PDI dimers were defined as

$$E_{form} = E_{dimer} - E_{monomer\,1} - E_{monomer\,2} \quad (1)$$

where E_{dimer} is the total energy of the dimer, $E_{monomer1}$ and $E_{monomer2}$ are the energy of different reduced states of PDI, individually.

The relative energies of different reduced states were defined as

$$E_{relative} = E_n - E_0 \quad (2)$$

where $E_{relative}$ is the relative energy of PDI molecules or $Ni(PDI)_2(DMF)_2$, E_n and E_0 are the total energy of different reduced states and neutral state of PDI or $Ni(PDI)_2(DMF)_2$, respectively.

The optimized ground structures were then used in time-dependent TDDFT calculations for the vertical excitation energies of clusters. In addition, orbital composition analysis and the charge transfer between ligands of the excited states were also performed using the Multiwfn program.[40−43] To better understand the transitions of the UV−vis spectrum, the excitation energies and oscillator strength of excited states of

https://doi.org/10.1021/acsami.4c01412
ACS Appl. Mater. Interfaces 2024, 16, 18194−18201

PDI were calculated. It can be seen from TDDFT calculations that the PDI exhibits two detectable absorption bands, called i and ii. An extremely strong absorption is located at 538.48 nm, which mainly originates from the HOMO → LUMO excitation, with the oscillator strength of 0.60. Another wide absorption at about 415.60 and 400.56 nm was calculated with the oscillator strength of 0.09 and 0.02, respectively.

RESULTS AND DISCUSSION

Design and Characterization of MOF. To increase the solubility of ligand in polar reagents,[44] we chose the nonplanar halognenlized PDI as the organic linker (Figure S3), and then PDI-based MOFs were synthesized in the presence of Ni^{2+} nodes via the solvothermal method. Structural analysis showed that the MOF material had the monoclinic space group $C\,2/c$ with a head-to-tail arrangement of PDI ligands (Figures 1a and S4). Due to nonplanar PDI molecules, adjacent PDI units interacted with a slipping angle of 40.53° (Figure 1b), which is a typical feature for J-dimers in frameworks.[45,46] The vertical distance between parallel aromatic planes was 5.74 Å (Figure 1c), resulting in relatively weak intrareticular electronic interactions.[47] The PXRD pattern of the MOF revealed distinct diffraction peaks at 3.7°, 7.3°, and 10.9°, which corresponded well with the simulated diffraction peaks (Figure 1d). After forming the framework, the vibrational absorption band of C═O at 1712 cm^{-1} decreased and blue-shifted compared to PDI ligand (Figure 1e). Furthermore, the MOF exhibited broad lamellar rectangular crystals (Figure S5) and homogeneous distribution of Ni, Cl, and N elements in the structure with the +2 valence state of Ni in the framework (Figures S6 and S7). Overall, PDI dimers were successfully incorporated into the framework, providing the possibilities for the stabilization of radical ions.

Electrochemical and ECL Properties of MOF. In the cathodic scanning, both PDI- and MOF-modified GCEs demonstrated three ECL peaks using 100 mM $S_2O_8^{2-}$ as coreactant at −0.3, −1.0, and −1.8 V (Figure 2a), which were denoted as ECL 0, ECL 1, and ECL 2, respectively.[48,49] CV test in acetonitrile clearly revealed three reduction peaks for both ligand and MOF (Figures 2b and S8), corresponding to three-step ECL emissions. Significantly, the ECL 2 intensity of the MOF showed 69.7-fold enhancement compared to the PDI ligand (Figure 2a). Unlike the anodic ECL (Figure S9), it was noteworthy that the intensity of ECL 2 for the MOF increased with first-half scanning and appeared as the peak in second-half scanning (Figure S10), indicating the accumulation of stable radicals during cathodic ECL scanning.

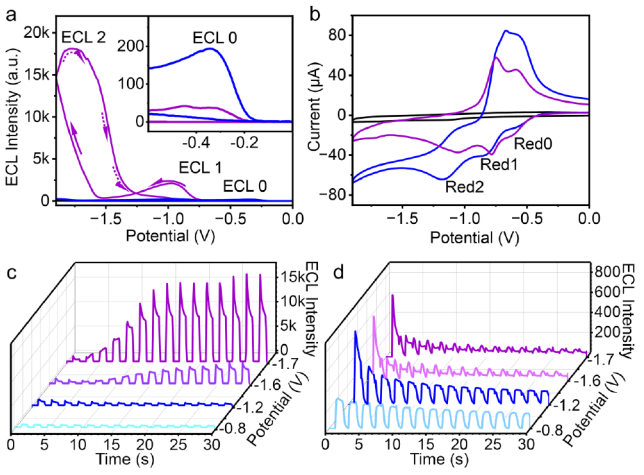

Figure 2. (A) ECL curves in the aqueous phase containing 100 mM $S_2O_8^{2-}$, and (b) CV curves in acetonitrile at bare electrode (black), MOF (purple), and PDI (blue). Inset: amplified ECL curves between 0 V and −0.6 V. ECL transients of (c) MOF and (d) PDI with 100 mM $S_2O_8^{2-}$ by cathodic stepping pulse from 0 V to −0.8, −1.2, −1.6, and −1.7 V (pulse time: 1 s).

Furthermore, we characterized the ECL behavior of the MOF with continuous CV scans in the presence of a coreactant. In contrast to ECL 1, which decreased, ECL 2 achieved an obvious enhancement in peak ECL intensity and a positive shift in peak ECL potential. This was attributed to the accumulation of free radical intermediates as the number of scan segments increased in the potential range of 0 to −1.7 V (Figures 3 and S11, S12). Significantly, when the potential

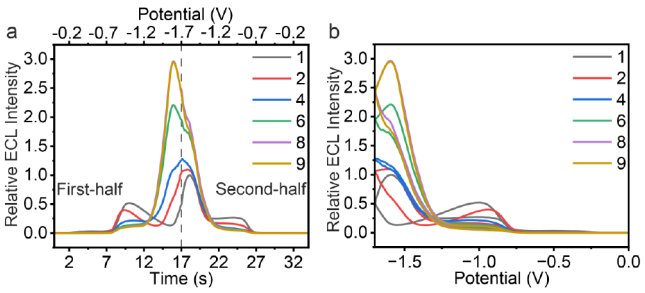

Figure 3. Dependence of relative ECL intensity divided by the initial intensity of ECL with MOF-modified GCE by using continuous CV scans (from 1 to 9 cycles) in the potential range of 0 to −1.7 V on (a) scanning time and (b) potentials in PBS containing 100 mM $S_2O_8^{2-}$.

dropped to −1.6 V, the ECL transients of MOF demonstrated a 16.8-fold enhancement of ECL intensity (Figures 2c and S13), suggesting self-accumulated ECL. By using the amperometric i−t method at different potentials, it was also observed that the ECL intensity of MOF at low potentials grew along with the scanning time, whereas the ECL signal dropped at high potentials (Figure S14). For individual ligands, Ni^{2+}, and Ni-gly, there was no ECL enhancement at low potential for either transient or continuous scanning (Figures 2d and S15−S17). The self-accumulated ECL of the MOF could be attributed to the formation of stable anion radicals in the framework at a more negative potential.

Stability of Free Radicals in Frameworks. We performed EPR tests to visually confirm the stability of radicals in frameworks. In dark, the single-electron signal intensity of MOF was ∼700-fold greater than that of the free ligand due to the framework's shielding effect (Figure S18a).[50] Under *in situ* light at 500 nm, the EPR signal of PDI ligand progressively grew and reached a plateau at 15 min, following with the rapid decline after turning off the light (Figure S18b). However, for MOF structure, the EPR signal kept constant in either dark or light irradiation due to the generation of saturated radicals during thermal synthesis (Figure 4a).[51] Moreover, the radical signal had no obvious decay after the light was turned off. Upon storage of the MOF in the dark, the EPR signal attenuation was only 3.8% for 5 days and 17.8% for one month (Figure 4b), demonstrating the ultrastability of free radicals in frameworks.

To explore the stability of anion−cation radicals, the annihilation process of transient ECL was examined using the stepping pulse (SP) method. A strong ECL signal occurred

https://doi.org/10.1021/acsami.4c01412
ACS Appl. Mater. Interfaces 2024, 16, 18194−18201

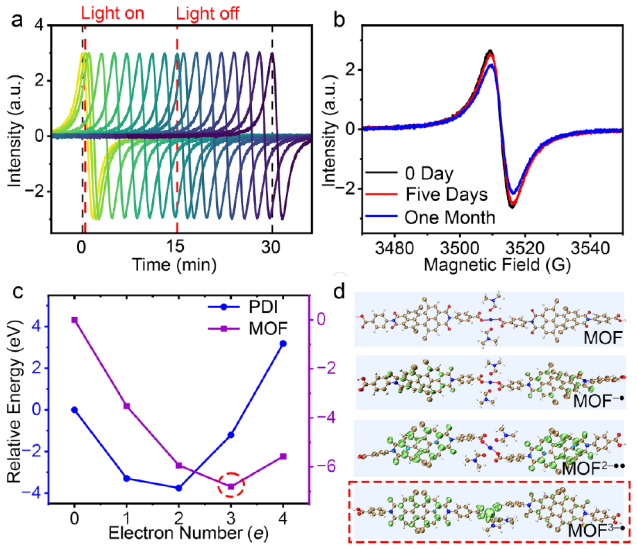

Figure 4. (a) *In situ* EPR spectra of solid MOF in light (500 nm) for 15 min and in dark. (b) EPR spectra of MOF preserved in dark conditions for different times. (c) Relative energies of PDI and MOF fragments after injection of different numbers of electrons. (d) Structure of MOF fragment and spin isodensity surfaces of MOF, $MOF^{-\bullet}$, $MOF^{2-\bullet\bullet}$, and $MOF^{3-\bullet}$ (isovalue = 0.002). Green and blue regions denote the populations of spin-α and spin-β electrons, respectively. $MOF^{-\bullet}$, $MOF^{2-\bullet\bullet}$, and $MOF^{3-\bullet}$ represent the injection of one, two, and three electrons into MOF, respectively.

after the first pulse cycle with the initial potential of −1.6 or −0.9 V, while no similar phenomenon was observed with the initial potential of +1.6 V, suggesting that anionic radicals were more stable than cationic radicals for MOF (Figure S19). Furthermore, DFT calculations were used to determine the relative stability of the PDI and MOF with different quantities of electrons. In comparison to the electrically neutral state, both the MOF and PDI tended to accept electrons to form lower energy systems. Upon electron injections, the energy of MOF sequentially decreased with the electron numbers, and reached the lowest energy at third reduction in the low-spin state (Figure 4c and Table S1), which was rationalized by the reduced spin density via electron spin pairing (Figure 4d).

ECL Emission of Ligand-Dimerized Frameworks. By analyzing the solid UV absorption spectra, the MOF had a band gap of 2.17 eV, suggesting it to be a typical semiconductor (Figure S20). Time-dependent DFT calculations indicated that there were two detectable absorption bands for the PDI ligand (Figure 5a), where the absorption at

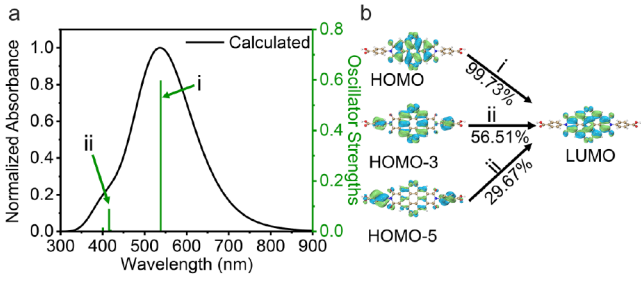

Figure 5. (a) Calculated solid UV−vis absorption spectrum of PDI and (b) MO isodensity surfaces in i and ii absorption bands of PDI. Green and blue regions denote the positive and negative orbital phases, respectively (isovalue = 0.02).

538.5 nm corresponded to the HOMO to LUMO leap. Meanwhile, the absorption at 415.6 nm had the contribution of two excited states, i.e., the HOMO−3 and HOMO−5 to LUMO leaps. Based on oscillator strengths, we found that the excited states of the PDI ligands were mainly contributed by HOMO to LUMO leaps (Figure 5b and Table S2). Moreover, the redshift of the liquid UV spectrum of MOF confirmed the presence of the dimerization structure in the framework with PDI molecule as the major chromophore unit (Figure S21).[52]

To further investigate the multistep ECL behavior of MOF, we performed ECL tests under different pH conditions (Figure 6a). The intensity of ECL 1 increased with the increase of pHs, which was attributed to the reduction of carbonyl groups in MOFs facilitated in high pHs (Figure S22).[53−55] Meanwhile, the intensity of ECL 2 remained constant in pH range from 5 to 9, since the electrons were mainly injected into perylene units (Figures 4d and 6d), leading to relatively stable radicals for self-accumulated ECL. The photoluminescence of free ligand in DMF showed two significant emission peaks at 550 and 610 nm (Figure S23). At the low concentration of PDI molecules in DMF, the emission mainly appeared at 550 nm due to the presence of PDI monomers. As the concentration of PDI increased, the emission at 550 nm decreased, and the emission at 610 nm gradually increased, corresponding to dimer emission at high concentrations (Figure 6c). By comparison with the photoluminescence of MOF and PDI, the ECL spectrum of the MOF was consistent with that of the PDI dimer centered at 610 nm (Figure 6b).

The dimerization energetics of PDI moieties in various reduced states were evaluated by DFT calculations. The spin density distribution exhibited that the unpaired electrons were delocalized at the center of the hydrazone nucleus of PDI in the dimer structure. The ligand with different reduced states can dimerize with neutral PDI to form dimers such as $(PDI)_2$, $(PDI)_2^{-\bullet}$, $(PDI)_2^{2-}$, $(PDI)_2^{2-\bullet\bullet}$, and $(PDI)_2^{3-\bullet}$, which were energetically favorable. Meanwhile, Coulomb repulsion was the cause of the high formation energies between negatively charged monomers. Obviously, $(PDI)_2^{-\bullet}$ and $(PDI)_2^{2-\bullet\bullet}$ have lower formation energies than $(PDI)_2$ (Table 1), which is ascribable to charge delocalization over PDI units.[29] When three electrons were injected, two of the electrons were spin-paired, leading to the spin density reduction (Figure 6d). $(PDI)_2^{3-\bullet}$ was energetically favorable due to a combination of excitonic coupling and charge transfer interactions in PDI dimers.[56] Based on the analysis above, MOF underwent a three-step reduction on the electrode surface, sequentially generating $(PDI)_2^{-\bullet}$, $(PDI)_2^{2-\bullet\bullet}$, and $(PDI)_2^{3-\bullet}$ with lower energies, which reacted with $SO_4^{\bullet-}$ to form excited states, individually, and produced self-accumulated ECL emissions, provided a promising methodology to understand ECL fundamentals.

CONCLUSION

In summary, we successfully designed an anion radical-stabilized MOF with ligand dimerization for self-accumulated ECL. Due to the distorted planar as well as head-to-tail arrangement of PDI ligands, the discrete J-dimer structure dominated in frameworks. Moreover, the large distance between parallel aromatic planes resulted in weak intrareticular electronic interactions in frameworks. DFT calculations identified that MOF tended to accept electrons, while the energetically favorable dimer structure in frameworks facilitated the delocalization of an unpaired electron over the whole

https://doi.org/10.1021/acsami.4c01412
ACS Appl. Mater. Interfaces 2024, 16, 18194−18201

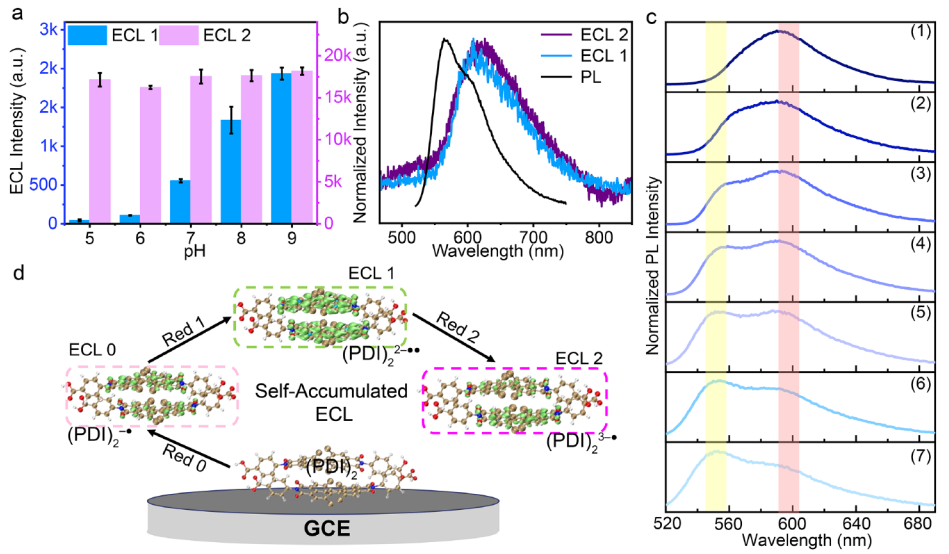

Figure 6. (a) Dependence of peak intensity of ECL 1 and ECL 2 on pHs. (b) PL and ECL spectra of MOFs. (c) PL spectra of PDI in DMF solution with concentrations of 1.0 (1), 0.5 (2), 0.2 (3), 0.1 (4), 0.05 (5), 0.025 (6), and 0.01 (7) mg mL^{-1}. (d) Schematic ECL mechanism via the accumulation of dimer-stabilized radicals. Spin isodensity surfaces of the dimerized PDI in MOF after injection of different electrons (isovalue = 0.002). Green and blue regions denote the populations of spin-α and spin-β electrons, respectively.

Table 1. DFT-Calculated Formation Energies for Different Reduced States of the PDI Dimers

monomer			dimer	formation energy (kcal/mol)
PDI	+	PDI	$(PDI)_2$	−36.79
$PDI^{-\bullet}$	+	PDI	$(PDI)_2^{-\bullet}$	−45.831
$PDI^{-\bullet}$	+	$PDI^{-\bullet}$	$(PDI)_2^{2-}$	−5.69
PDI^{2-}	+	PDI	$(PDI)_2^{2-}$	−67.61
$PDI^{2-\bullet\bullet}$	+	PDI	$(PDI)_2^{2-\bullet\bullet}$	−93.78
$PDI^{3-\bullet}$	+	PDI	$(PDI)_2^{3-\bullet}$	−109.98
PDI^{2-}	+	$PDI^{-\bullet}$	$(PDI)_2^{3-\bullet}$	24.44

PDI molecule and thus enhanced the stability of radical intermediates. Therefore, a significant enhancement of the ECL signal was achieved via the accumulation of free radical intermediates on the electrode surface. Indeed, free radicals in the designed frameworks can remain for one month. The ligand-dimerized frameworks not only illustrated the strategic use of ligand dimers in MOFs to stabilize radical ions for self-accumulated ECL but also gave a guideline for design of next-generation ECL nanoemitters.

■ ASSOCIATED CONTENT

Supporting Information

The Supporting Information is available free of charge at https://pubs.acs.org/doi/10.1021/acsami.4c01412.

Synthesis of ligand; ^1H NMR and mass spectra for PDI ligand; spatial structure of MOF and PDI ligand; additional characterization for material, CV and ECL data, photoluminescence and UV absorption spectra, EPR, and computational data (PDF)

■ AUTHOR INFORMATION

Corresponding Authors

Jing Ma − *Key Laboratory of Mesoscopic Chemistry, School of Chemistry and Chemical Engineering, Nanjing University, Nanjing 210023, P. R. China;* orcid.org/0000-0001-5848-9775; Phone: +86-25-89681922; Email: majing@nju.edu.cn; Fax: +86-25-89681922

Jianping Lei − *State Key Laboratory of Analytical Chemistry for Life Science, School of Chemistry and Chemical Engineering, Nanjing University, Nanjing 210023, P. R. China;* orcid.org/0000-0002-3594-180X; Email: jpl@nju.edu.cn

Authors

Qizhou Chen − *State Key Laboratory of Analytical Chemistry for Life Science, School of Chemistry and Chemical Engineering, Nanjing University, Nanjing 210023, P. R. China*

Yuming Gu − *Key Laboratory of Mesoscopic Chemistry, School of Chemistry and Chemical Engineering, Nanjing University, Nanjing 210023, P. R. China*

Haomin Fu − *State Key Laboratory of Analytical Chemistry for Life Science, School of Chemistry and Chemical Engineering, Nanjing University, Nanjing 210023, P. R. China*

Rengan Luo − *State Key Laboratory of Analytical Chemistry for Life Science, School of Chemistry and Chemical Engineering, Nanjing University, Nanjing 210023, P. R. China*

Da Zhu − *State Key Laboratory of Analytical Chemistry for Life Science, School of Chemistry and Chemical Engineering, Nanjing University, Nanjing 210023, P. R. China*

Pengfei Dong − *State Key Laboratory of Analytical Chemistry for Life Science, School of Chemistry and Chemical Engineering, Nanjing University, Nanjing 210023, P. R. China*

Huangxian Ju − *State Key Laboratory of Analytical Chemistry for Life Science, School of Chemistry and Chemical Engineering, Nanjing University, Nanjing 210023, P. R. China;* orcid.org/0000-0002-6741-5302

Complete contact information is available at: https://pubs.acs.org/10.1021/acsami.4c01412

Author Contributions

[§]Q.C., Y.G. and H.F. contributed equally to this work. The manuscript was written through contributions of all authors. All authors have given approval to the final version of the manuscript.

Notes

The authors declare no competing financial interest.

■ ACKNOWLEDGMENTS

We gratefully acknowledge the National Natural Science Foundation of China (22274071, 22234005, 22033004), the Natural Science Foundation of Jiangsu Province (BZ2021010), the Fundamental Research Funds for Central Universities (020514380280, 020514380297), the State Key Laboratory of Analytical Chemistry for Life Science (5431ZZXM2204), and the Jiangsu Provincial Excellent Postdoctoral Program (grant No. 2023ZB655).

■ REFERENCES

(1) Dong, J.; Lu, Y.; Xu, Y.; Chen, F.; Yang, J.; Chen, Y.; Feng, J. Direct Imaging of Single-Molecule Electrochemical Reactions in Solution. *Nature* **2021**, *596*, 244−249.

(2) Guo, W.; Ding, H.; Gu, C.; Liu, Y.; Jiang, X.; Su, B.; Shao, Y. Potential-Resolved Multicolor Electrochemiluminescence for Multiplex Immunoassay in a Single Sample. *J. Am. Chem. Soc.* **2018**, *140*, 15904−15915.

(3) Xia, H.; Zheng, X.; Li, J.; Wang, L.; Xue, Y.; Peng, C.; Han, Y.; Wang, Y.; Guo, S.; Wang, J.; et al. Identifying Luminol Electrochemiluminescence at the Cathode via Single-Atom Catalysts Tuned Oxygen Reduction Reaction. *J. Am. Chem. Soc.* **2022**, *144*, 7741−7749.

(4) Xu, W.; Wu, Y.; Wang, X.; Qin, Y.; Wang, H.; Luo, Z.; Wen, J.; Hu, L.; Gu, W.; Zhu, C. Bioinspired Single-Atom Sites Enable Efficient Oxygen Activation for Switching Anodic/Cathodic Electrochemiluminescence. *Angew. Chem., Int. Ed.* **2023**, *62* (29), No. e202304625.

(5) Beladi-Mousavi, S. M.; Salinas, G.; Bouffier, L.; Sojic, N.; Kuhn, A. Wireless Electrochemical Light Emission in Ultrathin 2D Nanoconfinements. *Chem. Sci.* **2022**, *13*, 14277−14284.

(6) Luo, R.; Zhu, D.; Ju, H.; Lei, J. Reticular Electrochemiluminescence Nanoemitters: Structural Design and Enhancement Mechanism. *Acc. Chem. Res.* **2023**, *56*, 1920−1930.

(7) Knezevic, S.; Bouffier, L.; Liu, B. H.; Jiang, D. C.; Sojic, N. Electrochemiluminescence Microscopy: from Single Objects to Living Cells. *Curr. Opin. Electrochem* **2022**, *35*, 101096.

(8) Liu, Y.; Zhang, H.; Li, B.; Liu, J.; Jiang, D.; Liu, B. H.; Sojic, N. Single Biomolecule Imaging by Electrochemiluminescence. *J. Am. Chem. Soc.* **2021**, *143*, 17910−17914.

(9) Carrara, S.; Arcudi, F.; Prato, M.; De Cola, L. Amine-Rich Nitrogen-Doped Carbon Nanodots as a Platform for Self-Enhancing Electrochemiluminescence. *Angew. Chem., Int. Ed.* **2017**, *56*, 4757−4761.

(10) Swanick, K. N.; Ladouceur, S.; Zysman-Colman, E.; Ding, Z. Self-Enhanced Electrochemiluminescence of an Iridium(III) Complex: Mechanistic Insight. *Angew. Chem., Int. Ed.* **2012**, *51*, 11079−11082.

(11) Zhu, D.; Zhang, Y.; Bao, S.; Wang, N.; Yu, S.; Luo, R.; Ma, J.; Ju, H.; Lei, J. Dual Intrareticular Oxidation of Mixed-Ligand Metal−Organic Frameworks for Stepwise Electrochemiluminescence. *J. Am. Chem. Soc.* **2021**, *143*, 3049−3053.

(12) Wang, N.; Gao, H.; Li, Y.; Li, G.; Chen, W.; Jin, Z.; Lei, J.; Wei, Q.; Ju, H. Dual Intramolecular Electron Transfer for In Situ Coreactant-Embedded Electrochemiluminescence Microimaging of Membrane Protein. *Angew. Chem., Int. Ed.* **2021**, *60*, 197−201.

(13) Luo, R.; Lv, H.; Liao, Q.; Wang, N.; Yang, J.; Li, Y.; Xi, K.; Wu, X.; Ju, H.; Lei, J. Intrareticular charge transfer regulated electrochemiluminescence of donor−acceptor covalent organic frameworks. *Nat. Commun.* **2021**, *12* (1), 6808.

(14) Li, Y.-J.; Cui, W.-R.; Jiang, Q.-Q.; Wu, Q.; Liang, R.-P.; Luo, Q.-X.; Qiu, J.-D. A General Design Approach toward Covalent Organic Frameworks for Highly Efficient Electrochemiluminescence. *Nat. Commun.* **2021**, *12* (1), 4735.

(15) Jin, Z.; Zhu, X.; Wang, N.; Li, Y.; Ju, H.; Lei, J. Electroactive Metal−Organic Frameworks as Emitters for Self-Enhanced Electrochemiluminescence in Aqueous Medium. *Angew. Chem., Int. Ed.* **2020**, *59*, 10446−10450.

(16) Zhang, J.-L.; Yao, L.-Y.; Yang, Y.; Liang, W.-B.; Yuan, R.; Xiao, D.-R. Conductive Covalent Organic Frameworks with Conductivity- and Pre-Reduction-Enhanced Electrochemiluminescence for Ultrasensitive Biosensor Construction. *Anal. Chem.* **2022**, *94*, 3685−3692.

(17) Zhang, S.; Ma, L.; Ma, W.; Chen, L.; Gao, K.; Yu, S.; Zhang, M.; Zhang, L.; He, G. Selenoviologen-Appendant Metallacycles with Highly Stable Radical Cations and Long-Lived Charge Separation States for Electrochromism and Photocatalysis. *Angew. Chem., Int. Ed.* **2022**, *61* (42), No. e202209054.

(18) Qiao, T.; Edwards, M. E.; Tang, X.; Yan, X.; Son, D. H. Efficient and Selective Photogeneration of Stable N-Centered Radicals via Controllable Charge Carrier Imbalance in Cesium Lead Halide Nanocrystals. *J. Am. Chem. Soc.* **2023**, *145*, 16862−16871.

(19) Borissov, A.; Chmielewski, P. J.; Gómez García, C. J.; Lis, T.; Stępień, M. Dinor[7]helicene and Beyond: Divergent Synthesis of Chiral Diradicaloids with Variable Open-Shell Character. *Angew. Chem., Int. Ed.* **2023**, *135* (38), No. e202309238.

(20) Schmidt, D.; Bialas, D.; Würthner, F. Ambient Stable Zwitterionic Perylene Bisimide-Centered Radical. *Angew. Chem., Int. Ed.* **2015**, *54*, 3611−3614.

(21) Schmidt, D.; Stolte, M.; Süß, J.; Liess, A.; Stepanenko, V.; Würthner, F. Protein-like Enwrapped Perylene Bisimide Chromophore as a Bright Microcrystalline Emitter Material. *Angew. Chem., Int. Ed.* **2019**, *58*, 13385−13389.

(22) Yang, F.; Li, R.; Wei, W.; Ding, X.; Xu, Z.; Wang, P.; Wang, G.; Xu, Y.; Fu, H.; Zhao, Y. Water-Soluble Doubly-Strapped Isolated Perylene Diimide Chromophore. *Angew. Chem., Int. Ed.* **2022**, *134* (20), No. e202202491.

(23) Liu, M.; Yang, X.; Sun, Q.; Wang, T.; Pei, R.; Yang, X.; Zhao, Y.; Zhao, L.; Frenking, G.; Wang, X. Lewis Acid-Mediated Radical Stabilization and Dynamic Covalent Bonding: Tunable, Reversible and Photocontrollable. *Angew. Chem., Int. Ed.* **2023**, *62* (20), No. e202300068.

(24) Zhang, A.; Jiang, W.; Wang, Z. Fulvalene-Embedded Perylene Diimide and Its Stable Radical Anion. *Angew. Chem., Int. Ed.* **2020**, *59*, 752−757.

(25) Yaghi, O. M.; Kalmutzki, M. J.; Diercks, C. S.. *Introduction to Reticular Chemistry: metal−Organic Frameworks and Covalent Organic Frameworks*; Wiley-VCH: Weinheim, Germany, 2019.

(26) Su, J.; Xu, N.; Murase, R.; Yang, Z.-M.; D'Alessandro, D. M.; Zuo, J.-L.; Zhu, J. Persistent Radical Tetrathiafulvalene-Based 2D Metal-Organic Frameworks and Their Application in Efficient Photothermal Conversion. *Angew. Chem., Int. Ed.* **2021**, *60*, 4789−4795.

(27) Hu, K.-Q.; Qiu, P.-X.; Zeng, L.-W.; Hu, S.-X.; Mei, L.; An, S.-W.; Huang, Z.-W.; Kong, X.-H.; Lan, J.-H.; Yu, J.-P.; et al. Solar-Driven Nitrogen Fixation Catalyzed by Stable Radical-Containing MOFs: Improved Efficiency Induced by a Structural Transformation. *Angew. Chem., Int. Ed.* **2020**, *59*, 20666−20671.

(28) Lü, B.; Chen, Y.; Li, P.; Wang, B.; Müllen, K.; Yin, M. Stable Radical Anions Generated from a Porous Perylenediimide Metal-Organic Framework for Boosting near-Infrared Photothermal Conversion. *Nat. Commun.* **2019**, *10*, 767.

(29) Kim, B.; Lee, J.; Chen, Y.-P.; Wu, X.-Q.; Kang, J.; Jeong, H.; Bae, S.-E.; Li, J.-R.; Sung, J.; Park, J. π-Stacks of Radical-Anionic Naphthalenediimides in a Metal-Organic Framework. *Sci. Adv.* **2022**, *8* (51), No. eade1383.

(30) Wang, H.; Xue, K.-F.; Yang, Y.; Hu, H.; Xu, J.-F.; Zhang, X. In Situ Hypoxia-Induced Supramolecular Perylene Diimide Radical

Anions in Tumors for Photothermal Therapy with Improved Specificity. *J. Am. Chem. Soc.* **2022**, *144*, 2360−2367.
(31) Zhao, Z.; Niu, F.; Li, P.; Wang, H.; Zhang, Z.; Meyer, G. J.; Hu, K. Visible Light Generation of a Microsecond Long-Lived Potent Reducing Agent. *J. Am. Chem. Soc.* **2022**, *144*, 7043−7047.
(32) Sebastian, E.; Philip, A. M.; Benny, A.; Hariharan, M. Null Exciton Splitting in Chromophoric Greek Cross (+) Aggregate. *Angew. Chem., Int. Ed.* **2018**, *57*, 15696−15701.
(33) Mohan Nalluri, S. K.; Zhou, J.; Cheng, T.; Liu, Z.; Nguyen, M. T.; Chen, T.; Patel, H. A.; Krzyaniak, M. D.; Goddard III, W. A.; Wasielewski, M. R.; et al. Discrete Dimers of Redox-Active and Fluorescent Perylene Diimide-Based Rigid Isosceles Triangles in the Solid State. *J. Am. Chem. Soc.* **2019**, *141*, 1290−1303.
(34) Nelson, A. P.; Farha, O. K.; Mulfort, K. L.; Hupp, J. T. Supercritical Processing as a Route to High Internal Surface Areas and Permanent Microporosity in Metal−Organic Framework Materials. *J. Am. Chem. Soc.* **2009**, *131*, 458−460.
(35) Deger, S. N.; Weishäupl, S. J.; Pöthig, A.; Fischer, R. A. A Perylenediimide-Based Zinc-Coordination Polymer for Photosensitized Singlet-Oxygen Generation. *Energies* **2022**, *15*, 2437.
(36) Frisch, M. J.; Trucks, G. W.; Schlegel, H. B.; Scuseria, G. E.; Robb, M. A.; Cheeseman, J. R.; Scalmani, G.; Barone, V.; Mennucci, B.; Petersson, G. A.; et al. Gaussian 16. In *Revision A.03*; Gaussian, Inc.: Wallingford, CT, USA, 2016.
(37) Becke, A. D. Density-functional thermochemistry. III. The role of exact exchange. *J. Chem. Phys.* **1993**, *98* (7), 5648−5652.
(38) Lee, C.; Yang, W. T.; Parr, R. G. Development of the Colle-Salvetti Correlation-Energy Formula into a Functional of the Electron Density. *Phys. Rev. B* **1988**, *37*, 785−789.
(39) Wadt, W. R.; Hay, P. J. Ab Initio Effective Core Potentials for Molecular Calculations. Potentials for Main Group Elements Na to Bi. *J. Chem. Phys.* **1985**, *82*, 284−298.
(40) Lu, T.; Chen, F. W. Multiwfn: A Multifunctional Wavefunction Analyzer. *J. Comput. Chem.* **2012**, *33*, 580−592.
(41) Lu, T.; Chen, F. W. Calculation of Molecular Orbital Composition. *Acta Chim. Sin.* **2011**, *69*, 2393−2406.
(42) Liu, Z. Y.; Lu, T.; Chen, Q. X. An Sp-Hybridized All-Carboatomic Ring, Cyclo[18]Carbon: Electronic Structure, Electronic Spectrum, and Optical Nonlinearity. *Carbon* **2020**, *165*, 461−467.
(43) Karabacak, M.; Cinar, M. FT-IR, FT-Raman, UV Spectra and DFT Calculations on Monomeric and Dimeric Structure of 2-Amino-5-bromobenzoic Acid. *Spectrochim. Acta, Part A* **2012**, *86*, 590−599.
(44) Zhou, J.; Liu, H.; Wang, W.; Li, T.; Li, Z.; Liu, Z.; Chen, Y.; Dong, Y.; Li, X. Influence of Core-Twisted Structure on Singlet Fission in Perylenediimide Film. *J. Photochem. Photobiol., A* **2023**, *438*, 114473.
(45) Chen, W.; Cheng, C.-A.; Cosco, E. D.; Ramakrishnan, S.; Lingg, J. G. P.; Bruns, O. T.; Zink, J. I.; Sletten, E. M. Shortwave Infrared Imaging with J-Aggregates Stabilized in Hollow Mesoporous Silica Nanoparticles. *J. Am. Chem. Soc.* **2019**, *141*, 12475−12480.
(46) Tian, D.; Qi, F.; Ma, H.; Wang, X.; Pan, Y.; Chen, R.; Shen, Z.; Liu, Z.; Huang, L.; Huang, W. Domino-like Multi-emissions across Red and Near Infrared from Solid-State 2-/2,6-aryl Substituted BODIPY Dyes. *Nat. Commun.* **2018**, *9* (1), 2688.
(47) Zhang, H.; Zhao, Z.; Turley, A. T.; Wang, L.; McGonigal, P. R.; Tu, Y.; Li, Y.; Wang, Z.; Kwok, R. T. K.; Lam, J. W. Y.; et al. Aggregate Science: from Structures to Properties. *Adv. Mater.* **2020**, *32* (36), 2001457.
(48) Zhang, W.; Song, Y.; Wang, Y.; Gong, Y.; Shang, L.; Ma, R.; Jia, L.; Xue, Q.; Du, Y.; He, S.; et al. Perylene Dianhydride and Perylene Diimide Luminophores Integrated with Gold Nanoparticles for Dual-Potential Electrochemiluminescence Ratiometric Immunosensors. *ACS Appl. Nano Mater.* **2021**, *4*, 683−690.
(49) Song, Y.; Zhang, W.; He, S.; Shang, L.; Ma, R.; Jia, L.; Wang, H. Perylene Diimide and Luminol as Potential-Resolved Electrochemiluminescence Nanoprobes for Dual Targets Immunoassay at Low Potential. *ACS Appl. Mater. Interfaces* **2019**, *11*, 33676−33683.
(50) Mi, Z.; Yang, P.; Wang, R.; Unruangsri, J.; Yang, W.; Wang, C.; Guo, J. Stable Radical Cation-Containing Covalent Organic Frameworks Exhibiting Remarkable Structure-Enhanced Photothermal Conversion. *J. Am. Chem. Soc.* **2019**, *141*, 14433−14442.
(51) Saha, S. Anion-Induced Electron Transfer. *Acc. Chem. Res.* **2018**, *51*, 2225−2236.
(52) Cravcenco, A.; Yu, Y.; Edhborg, F.; Goebel, J. F.; Takacs, Z.; Yang, Y.; Albinsson, B.; Börjesson, K. Exciton Delocalization Counteracts the Energy Gap: A New Pathway toward NIR-Emissive Dyes. *J. Am. Chem. Soc.* **2021**, *143*, 19232−19239.
(53) Lee, S. K.; Zu, Y.; Herrmann, A.; Geerts, Y.; Müllen, K.; Bard, A. J. Spectroscopy and Electrogenerated Chemiluminescence of Perylene, Terrylene, and Quaterrylene Diimides in Aprotic Solution. *J. Am. Chem. Soc.* **1999**, *121* (14), 3513−3520.
(54) Bai, Y.; Wang, Z.; Qin, N.; Ma, D.; Fu, W.; Lu, Z.; Pan, X. Two-Step Redox in Polyimide: Witness by In Situ Electron Paramagnetic Resonance in Lithium-ion Batteries. *Angew. Chem., Int. Ed.* **2023**, *62* (18), No. e202303162.
(55) Lu, Y.; Cai, Y.; Zhang, Q.; Chen, J. Insights into Redox Processes and Correlated Performance of Organic Carbonyl Electrode Materials in Rechargeable Batteries. *Adv. Mater.* **2022**, *34* (22), 2104150.
(56) Bornhof, A.-B.; Bauzá, A.; Aster, A.; Pupier, M.; Frontera, A.; Vauthey, E.; Sakai, N.; Matile, S. Synergistic Anion−$(\pi)_n$−π Catalysis on π-Stacked Foldamers. *J. Am. Chem. Soc.* **2018**, *140*, 4884−4892.

https://doi.org/10.1021/acsami.4c01412
ACS Appl. Mater. Interfaces 2024, 16, 18194−18201